MIMO Sliding Mode Trajectory Tracking Control of an Underwater Robot with Multidirectional Maneuverability *

Bhathiya Rathnayake

1 Abstract

Underwater robots capable of maneuvering in multiple directions are highly desired for inspection and surveillance tasks in complex underwater environments. In this project, we design a new underwater robotic vehicle (URV) with multidirectional mobility in the horizontal plane. The primary goal of this report is to develop a robust nonlinear controller to address the horizontal plane trajectory tracking problem of the presented URV. Based on multi-input-multi-output sliding mode control, we propose a trajectory tracking controller capable of mitigating the effects of hydrodynamic parameter uncertainties and handling coupled dynamics. Theoretical results which ensure the controller feasibility and closed-loop stability are provided. Simulation studies are conducted on dynamic models of the featured URV to illustrate the closed-loop system performance.

Contents

*Kindly note that the document is not peer reviewed.

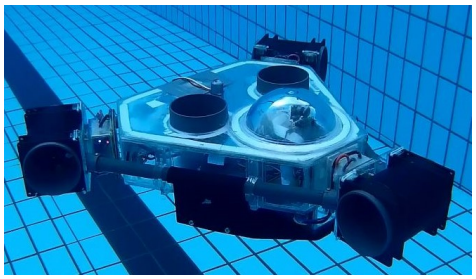

Fig. 1 *A Photograph of the URV taken at a trial in the swimming pool of University of Peradeniya, Sri Lanka.*

2 Introduction

In this report, we develop a robust nonlinear controller to solve the horizontal plane trajectory tracking problem of a new multidirectional underwater robotic vehicle (URV) (see Fig. 1). The robot is fully actuated in the horizontal plane and has been designed to operate at low speeds befitting inspection and surveillance tasks. The proposed controller is based on multi-input-multi-output (MIMO) SMC and is capable of withstanding hydrodynamic parameter uncertainties and coupled dynamics.

Notation: Bold uppercase letters denote matrices and bold lowercase letters stand for column vectors. For given scalar x, vector $\boldsymbol{x}$, and matrix $\boldsymbol{X}$, the following notations are adopted. $\boldsymbol{x}[i]$ is the i^{th} element of $\boldsymbol{x}$ and $\boldsymbol{X}[i,j]$ is the entry in the i^{th} row and j^{th} column of $\boldsymbol{X}$. The absolute value of x is denoted by $|x|$ and the 2-norm of $\boldsymbol{X}$ is written as $\|\boldsymbol{X}\|_2$. The term $\overrightarrow{|\boldsymbol{x}|}$ is a vector with its i^{th} element given by $|\boldsymbol{x}[i]|$ and $\widehat{x}$, $\widehat{\boldsymbol{x}}$, and $\widehat{\boldsymbol{X}}$ are the estimates of unknown x, $\boldsymbol{x}$, and $\boldsymbol{X}$ respectively. An $n \times n$ diagonal matrix $\boldsymbol{X}$ is written as $\boldsymbol{X} = \text{diag}(\lambda_1, \cdots, \lambda_n)$ where $\lambda_1, \cdots, \lambda_n$ are the diagonal elements.

3 Modeling of the URV

3.1 Design of the URV

The URV can maneuver in 3D space with multidirectional mobility in the horizontal plane. As shown in Fig. 2, the robot is equipped with five thrusters labeled as "T$_i$" for $i = 1, \cdots, 5$ and its framework is composed of four parts: a triangular main body, a spherical dome enclosing on-board processors, three

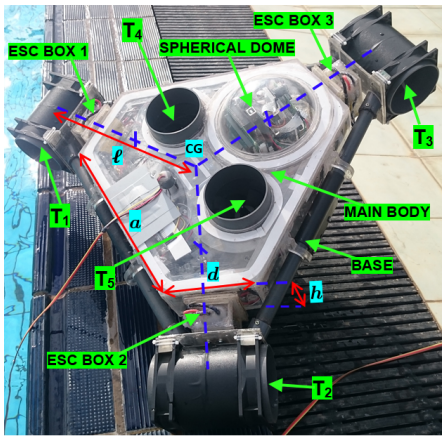

Fig. 2 *Isometric view of the URV*

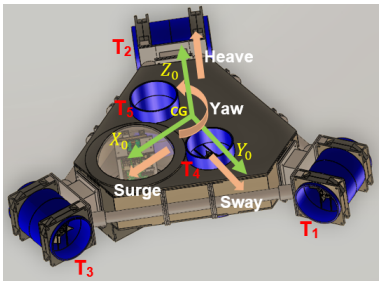

Fig. 3 *Controllable DOFs of the URV*

square boxes housing electronic speed controllers (ESCs), and a base supporting T_1,T_2, and T_3.

The DOFs supported by the URV are illustrated in Fig. 3 where $X_0Y_0Z_0$ is a moving frame attached to the robot. T_1,T_2, and T_3 control motions in X_0Y_0 plane, namely surge, sway, and yaw, whereas T_4 and T_5 control heave motion along Z_0 direction. Roll motion (rotation around X_0) is avoided for simplicity by ensuring that equal actuation signals are applied to T_4 and T_5 for all times. The major structure parameters and specifications of the robot are tabulated in Table 1. Since the buoyancy is approximately equal to the weight, the robot is neutrally buoyant in the water.

3.2 Dynamic Model of the URV

The motion along Z_0 direction is decoupled from the motions in X_0Y_0 plane and actuated independently. Thus, the control problem in Z_0 direction can be treated independently of that in X_0Y_0 plane. Since our focus is trajectory tracking control in the horizontal plane, the considered model in this paper is the 3-DOF model of the URV in X_0Y_0 plane. As shown in Fig. 4, the moving

Table 1: Geometrical and Physical Properties and Specifications of the URV

Parameters	Values
Dimensions of Main Body	
a	31.5 cm
d	14.1 cm
h	8 cm
Distance ℓ from center of gravity (CG) to line of action of force	34.5 cm
Weight	10.15 kgf
Moment of inertia around $Z_0(I_{z_0})$	0.22 kg.m^2
Buoyancy	10.3 kgf
Thrust force	
maximum	20 N
minimum	-15 N
Maximum operating depth	5 m

frame X_0Y_0 is attached to the center of gravity (CG) of the robot to simplify dynamic equations. XY is the earth frame which is stationary with respect to the earth and is used to describe the motion of the moving frame. The system of kinematic and dynamic equations of motion in the horizontal plane are given by [3]

$$\dot{\boldsymbol{\eta}} = \boldsymbol{R}(\varphi)\boldsymbol{\upsilon}, \tag{1a}$$

$$\boldsymbol{M}\dot{\boldsymbol{\upsilon}} + \boldsymbol{E}(\boldsymbol{\upsilon})\boldsymbol{\upsilon} + \boldsymbol{C}\boldsymbol{\upsilon} = \boldsymbol{B}\boldsymbol{\tau}. \tag{1b}$$

As depicted in Fig. 4, $\boldsymbol{\eta} = [x, y, \varphi]^T$ is the absolute position and orientation of the robot in the earth frame, $\boldsymbol{\upsilon} = [u, v, r]^T$ represents the velocities of the robot expressed in the moving frame, and $\boldsymbol{R} \in SO(3)$ is the rotation matrix between the earth frame and the moving frame written as

$$\boldsymbol{R} = \begin{bmatrix} \cos(\varphi) & -\sin(\varphi) & 0 \\ \sin(\varphi) & \cos(\varphi) & 0 \\ 0 & 0 & 1 \end{bmatrix}.$$

$\boldsymbol{M} \in \mathbb{R}^{3\times3}$ is the inertia matrix including hydrodynamic added inertia, $\boldsymbol{E} \in \mathbb{R}^{3\times3}$ is the Coriolis and the centripetal matrix, $\boldsymbol{C} \in \mathbb{R}^{3\times3}$ is the linear damping matrix, $\boldsymbol{B} \in \mathbb{R}^{3\times3}$ is the input matrix, and $\boldsymbol{\tau} = [\tau_1, \tau_2, \tau_3]^T \in \mathbb{R}^3$ is the thrust force vector in the moving frame. $\boldsymbol{M}$ and $\boldsymbol{C}$ are chosen to have diagonal structures as $\boldsymbol{M} = \text{diag}(m_1, m_2, m_3)$ and $\boldsymbol{C} = \text{diag}(c_1, c_2, c_3)$ because the effect of off-diagonal elements of these matrices on slow operating underwater vehicles is

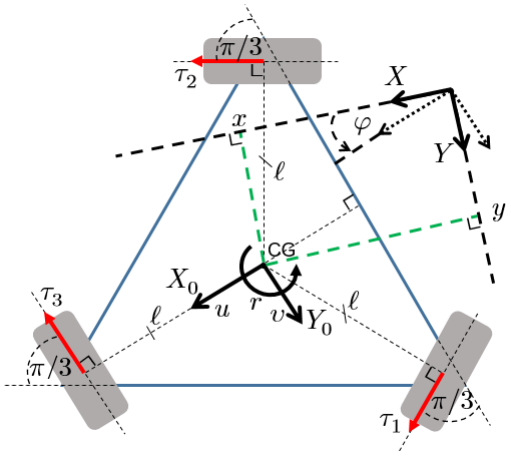

Fig. 4 *The URV in different coordinate frames in the horizontal plane*

small compared to that of diagonal elements [3]. Further, linear damping in $\boldsymbol{C}$ provides a fair approximation for hydrodynamic damping on vehicles operating at low speeds [4]. The matrix $\boldsymbol{E}$ is given by

$$\boldsymbol{E} = \begin{bmatrix} 0 & 0 & -m_2 v \\ 0 & 0 & m_1 u \\ m_2 v & -m_1 u & 0 \end{bmatrix}.$$

The terms m_1, m_2, and m_3 in $\boldsymbol{M}$ and $\boldsymbol{E}$ known as inertia terms are calculated as $m_1 = m - X_{\dot{u}}$, $m_2 = m - Y_{\dot{v}}$, and $m_3 = I_{z_0} - N_{\dot{r}}$ where m is the mass of the robot, I_{z_0} is its moment of inertia around Z_0 axis, and $X_{\dot{u}}$, $Y_{\dot{v}}$, and $N_{\dot{r}}$ stand for added inertia coefficients in each DOF [3]. c_1, c_2, and c_3 in $\boldsymbol{C}$ represent linear drag coefficients in each DOF. Referring to Fig. 4, we can express $\boldsymbol{B}$ as

$$\boldsymbol{B} = \begin{bmatrix} \sqrt{3}/2 & \sqrt{3}/2 & 0 \\ 1/2 & -1/2 & -1 \\ -\ell & \ell & -\ell \end{bmatrix},$$

where ℓ is the perpendicular distance from the CG to the line of action of force.

The dynamic model derived here contains many uncertain parameters such as added inertia and drag coefficients which should be taken into account in controller design. The estimates of the added inertia coefficients were obtained using the finite volume method for added mass computing [5] and simulation in ANSYS ICEM computational fluid dynamics software (CFD): $\widehat{X}_{\dot{u}} = -14.05$ kg, $\widehat{Y}_{\dot{v}} = -11.65$ kg, and $\widehat{N}_{\dot{r}} = 0.02$ kg.m^2 from which the estimates of the inertia terms were calculated as $\widehat{m}_1 = 24.2$ kg, $\widehat{m}_2 = 21.8$ kg, and $\widehat{m}_3 = 0.2$ kg.m^2. The estimates of the drag coefficients were obtained by simulation using ANSYS CFX CFD: $\widehat{c}_1 = 38.8$ kg/s, $\widehat{c}_2 = 29.4$ kg/s, and $\widehat{c}_3 = 3.1$ kg.m^2/s.

4 Sliding Mode Control (SMC) for a Class of Fully Actuated Robots

SMC is a nonlinear control strategy which is robust to modeling inaccuracies. This allows us to proceed with controller design without precise system models. However, the discontinuity in the control law leads to the widely known '*chattering*' phenomenon which is undesirable [1]. Smoothing out the control discontinuity in a thin boundary layer can suppress chattering at the expense of perfect tracking [6].

It can easily be seen from (1) that the dynamics (both motions and actuations) in different DOFs in X_0Y_0 plane are coupled. Hence, the use of independent single-input-single-output (SISO) sliding mode controllers for motion control in individual DOFs may not guarantee the overall stability of the closed-loop system. Unstable dynamics in a particular DOF can trigger instability in another DOF due to their inter-dependencies (consider a nonlinear system having properties like finite escape time). This motivates us to consider the MIMO version of SMC [2, 6] which permits coupling between DOFs.

4.1 MIMO SMC Design

Let's consider a fully actuated, generic n-DOF system

$$\ddot{\boldsymbol{x}} = \boldsymbol{h} + \boldsymbol{q} + \boldsymbol{A}\boldsymbol{\tau}, \tag{2}$$

where $\boldsymbol{x}$, $\boldsymbol{h}$, $\boldsymbol{q}$, $\boldsymbol{\tau} \in \mathbb{R}^n$ and $\boldsymbol{A} \in \mathbb{R}^{n\times n}$ with dynamic behavior in the i^{th} DOF captured by

$$\ddot{x}_i = h_i + q_i + \sum_{j=1}^{n} A_{ij}\tau_j, \tag{3}$$

$\forall i \in \mathbb{M} = \{1, \cdots, n\}$. The developments in this section are valid for any robotic system complying with (2) and (3) whose terms are defined as follows: $\boldsymbol{x}[i] = x_i$ is the position information in the i^{th} DOF, $\boldsymbol{h}[i] = h_i(x_1, \dot{x}_1, \cdots, x_n, \dot{x}_n) : \mathbb{R}^{2n} \to \mathbb{R}$ and $\boldsymbol{A}[i,j] = A_{i,j}(x_1, \dot{x}_1, \cdots, x_n, \dot{x}_n) : \mathbb{R}^{2n} \to \mathbb{R}$ are unknown due to parametric uncertainties, but are continuous nonlinear functions, $\boldsymbol{q}[i] = q_i(x_1, \dot{x}_1, \cdots, x_n, \dot{x}_n) : \mathbb{R}^{2n} \to \mathbb{R}$ is a known continuous nonlinear function, and $\boldsymbol{\tau}[j] = \tau_j$ is the control signal for the j^{th} DOF.

Let $y_i : t[0, \infty) \to \mathbb{R}$ be the reference trajectory which x_i should track. The goal is to find a control law $\boldsymbol{\tau}$ such that in the presence of parametric uncertainties, the tracking errors $e_i = x_i - y_i \in \mathbb{R}, \forall i \in \mathbb{M}$ converge to a neighborhood of zero which can be made arbitrarily small with bounded closed-loop dynamics.

Let S_i be a sliding surface defined in the error state space by the equation $s_i(e_i, \dot{e}_i) = 0$ with $s_i : \mathbb{R}^2 \to \mathbb{R}$ satisfying

$$s_i = \dot{e}_i + \lambda_i e_i, \tag{4}$$

where $\lambda_i, \forall i \in \mathbb{M}$ is a strictly positive constant. Here s_i can be interpreted as a measure of the distance from the current error states e_i and $\dot{e}_i$ to the sliding surface S_i.

Remark 1: If s_i can be brought to and regulated at zero for $t \geq t_0$ where t_0 is the time instant when s_i hits S_i, it can be seen from (4) that the dynamics of e_i is thereafter characterized by a linear, first order homogeneous differential equation which makes $e_i \to 0$ exponentially at a rate of λ_i.

Here we shall make the following assumptions.

Assumption 1: x_i and $\dot{x}_i$ are available.

Assumption 2: y_i is at least once differentiable in time and $\ddot{y}_i$ is available with known bounds.

Assumption 1 and *2* allows a unique s_i to be found for all times without any ambiguity. We can easily verify using (3) and (4) that the time derivative of s_i is given by

$$\dot{s}_i = h_i + q_i - \ddot{y}_i + \lambda_i \dot{e}_i + \sum_{j=1}^{n} A_{ij}\tau_j. \tag{5}$$

Let's combine the n equations which stem from (5) as $i \in \mathbb{M}$ to form the vector equation

$$\dot{\boldsymbol{s}} = \boldsymbol{h} + \boldsymbol{q} - \boldsymbol{\gamma} + \boldsymbol{\Lambda}\dot{\boldsymbol{e}} + \boldsymbol{A}\boldsymbol{\tau}, \tag{6}$$

with $\boldsymbol{s} = [s_1, \cdots, s_n]^T$, $\boldsymbol{\gamma} = [\ddot{y}_1, \cdots, \ddot{y}_n]^T$, $\boldsymbol{e} = [e_1, \cdots, e_n]^T$, and $\boldsymbol{\Lambda} = \text{diag}(\lambda_1, \cdots, \lambda_n)$.

Regarding the derivation of the control law, the following assumptions should also be made.

Assumption 3: The unknown h_i is bounded by a known continuous nonlinear function $\boldsymbol{\delta h}[i] = \delta h_i(x_1, \dot{x}_1, \cdots, x_n, \dot{x}_n) : \mathbb{R}^{2n} \to \mathbb{R}$ such that $|h_i - \widehat{h}_i| \leq \delta h_i$.

Assumption 4: The matrix $\boldsymbol{A}$ and its estimate $\widehat{\boldsymbol{A}}$ are invertible and $\boldsymbol{A} = \widehat{\boldsymbol{A}}$ in the absence parametric uncertainties. As proposed in [6], $\boldsymbol{A}$ is chosen to have the form $\boldsymbol{A} = (\boldsymbol{I} + \boldsymbol{\Delta})\widehat{\boldsymbol{A}}$ where $\boldsymbol{I} \in \mathbb{R}^{n\times n}$ is the identity matrix and unknown $\boldsymbol{\Delta} \in \mathbb{R}^{n\times n}$ captures $\boldsymbol{A}$'s uncertainties. $\boldsymbol{\Delta}[i,j] = \Delta_{ij}(x_1, \dot{x}_1, \cdots, x_n, \dot{x}_n) : \mathbb{R}^{2n} \to \mathbb{R}$ is bounded by a known $D_{ij}(x_1, \dot{x}_1, \cdots, x_n, \dot{x}_n) : \mathbb{R}^{2n} \to \mathbb{R}$ such that $0 \leq |\Delta_{ij}| \leq D_{ij}, \forall i, j \in \mathbb{M}$ where both Δ_{ij} and D_{ij} are continuous nonlinear functions. The matrix $\boldsymbol{D}$ with $\boldsymbol{D}[i,j] = D_{ij}$ has its maximum singular value less than one, i.e., $\|\boldsymbol{D}\|_2 < 1$.

Remark 2: The n-DOF system in (2) is fully actuated meaning that rank of $\boldsymbol{A} = n$. So, $\boldsymbol{A}$ should remain invertible over all possible A_{ij} for all times despite the parametric uncertainties, otherwise some states may not be controllable.

Now, let the feedback control law be chosen as

$$\boldsymbol{\tau} = \widehat{\boldsymbol{A}}^{-1}(\boldsymbol{f} - \boldsymbol{\Psi}\boldsymbol{k}), \tag{7a}$$

$$\boldsymbol{f} = -\widehat{\boldsymbol{h}} - \boldsymbol{q} + \boldsymbol{\gamma} - \boldsymbol{\Lambda}\dot{\boldsymbol{e}}, \tag{7b}$$

$$\boldsymbol{k} = (\boldsymbol{I} - \boldsymbol{D})^{-1}(\boldsymbol{\delta h} + \boldsymbol{D}\overrightarrow{|\boldsymbol{f}|} + \boldsymbol{\mu}), \tag{7c}$$

where $\boldsymbol{k} = [k_1, \cdots, k_n]^T$ which is the control gain vector, $\widehat{\boldsymbol{h}} = [\widehat{h}_1, \cdots, \widehat{h}_n]^T$, $\boldsymbol{\mu} = [\mu_1, \cdots, \mu_n]^T$ whose elements are tunable, but strictly positive, and

$$\boldsymbol{\Psi} = \mathrm{diag}\big(\mathrm{sat}(s_1/\phi_1), \cdots, \mathrm{sat}(s_n/\phi_n)\big).$$

Here, $\mathrm{sat}(s_i/\phi_i)$ is defined as

$$\mathrm{sat}(s_i/\phi_i) = \begin{cases} s_i/\phi_i, & \text{if } |s_i| \leq \phi_i \\ -1, & \text{if } s_i < -\phi_i \\ 1. & \text{if } s_i > \phi_i \end{cases} \tag{8}$$

$\phi_i > 0$ is the thickness of the boundary layer L_i associated with the sliding surface S_i. Hereinafter, s_i is called to be inside L_i if $|s_i| \leq \phi_i$ and outside L_i if $|s_i| > \phi_i$. It should be noted that $(\boldsymbol{I} - \boldsymbol{D})^{-1}$ in (7c) always exists as $\|\boldsymbol{I}\|_2 = 1 > \|\boldsymbol{D}\|_2$ following *Assumption 4*.

Remark 3: Instead of (8), conventional SMC uses the inherently discontinuous signum function which triggers undesirable chattering. The adoption of (8) smooths out the control discontinuity inside the boundary layer L_i and can suppress chattering. However, this alters perfect tracking into tracking up to a guaranteed precision [6].

Remark 4: If $\boldsymbol{f}[i] = f_i$ and $\boldsymbol{U}[i,j] = U_{ij}$ where $\boldsymbol{U} = \widehat{\boldsymbol{A}}^{-1}$, we note from (7a) that $\tau_i = \sum_{j=1}^{n} \big(U_{ij} f_j - k_j U_{ij}\, \mathrm{sat}(s_j/\phi_j)\big)$. The term $U_{ij}\, \mathrm{sat}(s_j/\phi_j)$ is weighted by a time varying term k_j. So, τ_i can be considered as a sum of weighted functions of states in all DOFs. This allows τ_i to adapt according to the dynamics of the overall system. In contrast, an appropriate independent SISO SMC control law for a particular DOF is unaware of the dynamic conditions in other DOFs which is not favorable for coupled MIMO systems.

We shall establish the convergence properties and the global stability of the closed-loop system under the control law (7) in *Theorem 1* using *Lemma 1-3*.

Lemma 1: For a nonnegative square matrix $\boldsymbol{H} \in \mathbb{R}^{n \times n}$, the largest real eigenvalue ρ_{max} is nonnegative. Furthermore, if $\rho > \rho_{max}$, and all the elements of $\boldsymbol{w} \in \mathbb{R}^n$ are nonnegative,

$$(\boldsymbol{I} - \rho^{-1}\boldsymbol{H})\boldsymbol{g} = \boldsymbol{w}, \tag{9}$$

yields a unique solution to $\boldsymbol{g}$ whose elements are nonnegative [6].

Lemma 2: Consider $a_1, a_2, \cdots, a_n \geq 0$. Then, we have $\sqrt{\sum_{i=1}^{n} a_i} \leq \sum_{i=1}^{n} \sqrt{a_i}$. The equality holds when at most one of a_i is nonzero.

Proof: For $n = 1$, it is apparent that the equality holds. For n=2,

$$\begin{aligned} \sqrt{a_1} + \sqrt{a_2} &= \sqrt{\big(\sqrt{a_1} + \sqrt{a_2}\big)^2} = \sqrt{a_1 + a_2 + 2\sqrt{a_1 a_2}} \\ &\geq \sqrt{a_1 + a_2}, \end{aligned}$$

and the equality holds if at most one of a_1 and a_2 are nonzero. Hence, we can write that

$$\begin{aligned}\sqrt{\sum_{i=1}^{n} a_i} &= \sqrt{a_1 + \sum_{i=2}^{n} a_i} \\ &\leq \sqrt{a_1} + \sqrt{\sum_{i=2}^{n} a_i} \leq \cdots \leq \sqrt{a_1} + \cdots + \sqrt{a_n} \\ &= \sum_{i=1}^{n} \sqrt{a_i}.\end{aligned}$$

By arguing in the same manner as for $n = 2$, it can be proven that the equality holds when at most one of a_i is nonzero.

Lemma 3: For an s_i trajectory which enters the corresponding boundary layer L_i at $t = t_0$ and thereafter remains inside, the error states e_i and $\dot{e}_i$ stay bounded for $t \geq t_0$ if $e_i(t_0)$ is finite. Further, as $t \to \infty$, e_i and $\dot{e}_i$ converge inside $|e_i| \leq \phi_i/\lambda_i$ and $|\dot{e}_i| \leq 2\phi_i$ respectively.

Proof: Inside the boundary layer L_i, we have $|s_i| \leq \phi_i$ which can alternatively be written as $-\phi_i \leq s_i \leq \phi_i$. So, it follows from (4) that

$$-\phi_i \leq \dot{e}_i + \lambda_i e_i \leq \phi_i, \tag{10}$$

which we multiply by $\exp(\lambda_i t)$ to obtain

$$-\phi_i \exp(\lambda_i t) \leq (\dot{e}_i + \lambda_i e_i) \exp(\lambda_i t) \leq \phi_i \exp(\lambda_i t).$$

Then, we can write that

$$-\phi_i \exp(\lambda_i t) \leq \frac{d\big(e_i \exp(\lambda_i t)\big)}{dt} \leq \phi_i \exp(\lambda_i t).$$

Assuming that $|s_i| \leq \phi_i, \forall t \geq t_0$, let's integrate the above between t_0 and t which yields

$$e_i \geq -\frac{\phi_i}{\lambda_i} + \Big(\frac{\phi_i}{\lambda_i} + e_i(t_0)\Big) \exp(-\lambda_i t),$$

and

$$e_i \leq \frac{\phi_i}{\lambda_i} - \Big(\frac{\phi_i}{\lambda_i} - e_i(t_0)\Big) \exp(-\lambda_i t), \quad \forall t \geq t_0.$$

Using this result along with (10), we can verify that

$$\dot{e}_i \geq -2\phi_i + \lambda_i \Big(\frac{\phi_i}{\lambda_i} - e_i(t_0)\Big) \exp(-\lambda_i t),$$

and

$$\dot{e}_i \leq 2\phi_i - \lambda_i \Big(\frac{\phi_i}{\lambda_i} + e_i(t_0)\Big) \exp(-\lambda_i t), \quad \forall t \geq t_0.$$

Since $\exp(-\lambda_i t)$ is positive and decreasing, e_i and $\dot{e}_i$ can be concluded to be bounded if $e_i(t_0)$ is finite. Further, as $t \to \infty$, we have $-\frac{\phi_i}{\lambda_i} \leq e_i \leq \frac{\phi_i}{\lambda_i}$ and $-2\phi_i \leq \dot{e}_i \leq 2\phi_i$.

Remark 5: Since we favor tracking errors to be as small as possible, according to *Lemma 3*, it is cautious to keep ϕ_i/λ_i small. On the other hand, in order to suppress chattering, we should choose ϕ_i sufficiently large [6]. So, it is intuitive to choose large values for λ_i. However, if λ_i is chosen to be very large, we can infer from (4) and (5) that when $|\dot{e}_i|$ is sufficiently large and $s_i\dot{e}_i > 0$, $|\sum_{j=1}^{n} A_{ij}\tau_j|$ may need to generate extremely large values to ensure $s_i\dot{s}_i < 0$ because we desire s_i to reach zero as implied in *Remark 1*. This increases the risk of actuator saturation. Therefore, the choice of appropriate ϕ_i and λ_i is a trade-off between suppression of chattering, minimizing tracking errors and reducing the risk of actuator saturation. Later, we shall see the impact of λ_i on the convergence times of s_i trajectories.

Theorem 1: Let the fully actuated n-DOF system be given by (2). Subject to *Assumption 1-4*, the controller defined in (7) guarantees the finite time convergence of s_i to the boundary layer $L_i, \forall i \in \mathbb{M}$ and ensures the global closed-loop stability.

Proof: Let's construct a Lyapunov function $V : \mathbb{R}^n \to \mathbb{R}$

$$V = \frac{1}{2}\boldsymbol{l}^T\boldsymbol{l} = \frac{1}{2}\sum_{i=1}^{n} {l_i}^2, \tag{11}$$

where l_i is given by

$$l_i = s_i - \phi_i \,\mathrm{sat}(s_i/\phi_i). \tag{12}$$

Here l_i can be interpreted as a measure of the signed distance from the boundary layer L_i to s_i in the i^{th} DOF. The time derivative of V is written as

$$\dot{V} = \boldsymbol{l}^T\dot{\boldsymbol{l}} = \sum_{i=1}^{n} l_i\dot{l}_i. \tag{13}$$

We notice from (8) and (12) that inside L_i, $l_i = 0$, and $\dot{l}_i = 0$. Outside L_i, $l_i = s_i - \phi_i > 0$ when $s_i > \phi_i$, whereas $l_i = s_i + \phi_i < 0$ when $s_i < -\phi_i$ and $\dot{l}_i = \dot{s}_i$ for both cases. While every s_i is inside its L_i, both V and $\dot{V}$ are zero. Let's consider the situation when s_j in the j^{th} DOF is outside L_j. The control law (7) is applied to (6). Based on *Assumption 4*, we have $\boldsymbol{A}\widehat{\boldsymbol{A}}^{-1} = \boldsymbol{I} + \boldsymbol{\Delta}$. Using this result, it can be verified that (6) yields

$$\dot{\boldsymbol{s}} = \boldsymbol{h} - \widehat{\boldsymbol{h}} - \boldsymbol{\Psi}\boldsymbol{k} + \boldsymbol{\Delta}(\boldsymbol{f} - \boldsymbol{\Psi}\boldsymbol{k}). \tag{14}$$

The equation which corresponds to the j^{th} DOF in (14) can be obtained as

$$\begin{aligned}\dot{s}_j =& h_j - \widehat{h}_j - (1 + \Delta_{jj})k_j \,\mathrm{sat}(s_j/\phi_j) \\ &+ \sum_{i=1}^{n} \Delta_{ji} f_i - \sum_{i \neq j}^{n} \Delta_{ji} k_i \,\mathrm{sat}(s_i/\phi_i).\end{aligned}$$

Noting that $l_j \neq 0$ and $\text{sat}(s_j/\phi_j) = \pm 1$ for $l_j \gtrless 0$, multiplying both sides by l_j yields

$$\begin{aligned} l_j \dot{s}_j =& (h_j - \widehat{h}_j) l_j - (1 + \Delta_{jj}) k_j |l_j| \\ &+ \sum_{i=1}^{n} \Delta_{ji} f_i l_j - \sum_{i \neq j}^{n} \Delta_{ji} k_i \,\text{sat}(s_i/\phi_i) l_j. \end{aligned} \tag{15}$$

Evoking the existence of $(\boldsymbol{I} - \boldsymbol{D})^{-1}$, we write from (7c) that

$$(\boldsymbol{I} - \boldsymbol{D})\boldsymbol{k} = \boldsymbol{\delta h} + \boldsymbol{D}\overrightarrow{|\boldsymbol{f}|} + \boldsymbol{\mu}. \tag{16}$$

For any square matrix $\boldsymbol{Z}$, the largest singular value of the matrix, i.e., $\|\boldsymbol{Z}\|_2$ dominates all the absolute values of its eigenvalues. So, following that $\|\boldsymbol{D}\|_2 < 1$ from *Assumption 4*, we can conclude that $|\rho_{max}| < 1$ where ρ_{max} is the largest real eigenvalue of $\boldsymbol{D}$. As stated in *Assumption 4*, all the elements of $\boldsymbol{D}$ are nonnegative. Hence considering *Lemma 1*, we have $\rho_{max} \geq 0$. We also observe that the right hand side of (16) is a vector whose elements are positive. This makes (16) equivalent to (9) with $\rho = 1$. Thus, adhering to *Lemma 1*, (16) yields a unique $\boldsymbol{k}$ with all the elements being nonnegative. Isolating the equation for j^{th} DOF in (16), we can obtain

$$0 = \delta h_j - (1 - D_{jj}) k_j + \sum_{i=1}^{n} D_{ji} |f_i| + \sum_{i \neq j}^{n} D_{ji} k_i + \mu_j.$$

Let's multiply both sides by $|l_j|$ and subtract from (15).

$$\begin{aligned} l_j \dot{s}_j =& -\left(\delta h_j |l_j| - (h_j - \widehat{h}_j) l_j\right) - (D_{jj} + \Delta_{jj}) k_j |l_j| \\ &- \sum_{i=1}^{n} \left(D_{ji} |f_i l_j| - \Delta_{ji} f_i l_j\right) - \sum_{i \neq j}^{n} \left(D_{ji} k_i |l_j| \right. \\ &\left. + \Delta_{ji} k_i \,\text{sat}(s_i/\phi_i) l_j\right) - \mu_j |l_j|. \end{aligned} \tag{17}$$

Using the result that $k_i \geq 0, \forall i \in \mathbb{M}$ along with *Assumption 3* and *4* and noting that $|\,\text{sat}(s_i/\phi_i)| \leq 1, \forall i \in \mathbb{M}$, we can observe that (17) satisfies $l_j \dot{s_j} \leq -\mu_j |l_j|$. Recalling $\dot{l}_j = \dot{s}_j$ for s_j outside L_j, we have $l_j \dot{l}_j \leq -\mu_j |l_j|$. In general, with s_j being anywhere (inside or outside L_j), $l_j \dot{l}_j \leq -\mu_j |l_j| \leq 0$ because $l_j = 0$ when s_j is inside L_j. So, with an arbitrary number of s_i being outside L_i, $\dot{V}$ always satisfies

$$\dot{V} = \sum_{i=1}^{n} l_i \dot{l}_i \leq -\sum_{i=1}^{n} \mu_i |l_i| \leq 0. \tag{18}$$

It follows from (11) and (18) that $V \geq 0$ and $V(t) \leq V(0)$ respectively. These make l_i bounded which in turn makes s_i bounded, $\forall i \in \mathbb{M}$ due to (12). So, we can admit from (4) that all the states (both system and error states) are bounded which makes the control inputs given by (7) are bounded as well.

Further, considering *Assumption 2* and (5), it can be verified that every $\dot{s}_i$ is also bounded indicating the boundedness of $\dot{l}_i$. Therefore, according to the Barbalat's Lemma, it follows that $\lim_{t\to\infty} \dot{V} = 0$. At $\dot{V} = 0$, every l_i should have approached zero, i.e., every s_i should have converged to the corresponding boundary layer L_i making $V = 0$ to remain consistent with (18).

Next, we prove that the convergence is achieved within finite time. We have from (18) that

$$\dot{V} \leq -\sum_{i=1}^{n} \mu_i |l_i| \leq -\mu_{min} \sum_{i=1}^{n} |l_i|,$$

where μ_{min} is the minimum among $\mu_i, \forall i \in \mathbb{M}$. Referring to *Lemma 2* and (11) we can write that

$$\dot{V} \leq -\mu_{min} \sum_{i=1}^{n} |l_i| \leq -\mu_{min} \sqrt{\sum_{i=1}^{n} |l_i|^2} = -\mu_{min} \sqrt{2V}.$$

Thus, we have $\dot{V}/\sqrt{V} \leq -\sqrt{2}\mu_{min}$ which we integrate between 0 and t to obtain $t \leq \sqrt{2}\Big(\sqrt{V(0)} - \sqrt{V(t)}\Big)/\mu_{min}$. If t_r denotes the time at which V reaches zero, we have

$$t_r \leq \sqrt{2V(0)}/\mu_{min} = \sqrt{\sum_{i=1}^{n} l_i^2(0)}/\mu_{min}, \tag{19}$$

indicating the finite time convergence of all s_i to the corresponding L_i. Further, it follows from *Lemma 3* that the error states e_i and $\dot{e}_i$ converge inside $|e_i| \leq \phi_i/\lambda_i$ and $|\dot{e}_i| \leq 2\phi_i$ respectively as $t \to \infty$. This ensures the global stability of the closed-loop system and completes the proof.

Remark 6: We observe from (19) that the elements of $\boldsymbol{\mu}$ contribute to setting an upper bound for t_r. Since it is desirable that system states converge on the sliding surface at the earliest time possible, it's intuitive to choose large values for μ_i in $\boldsymbol{\mu}$. However, it follows from (7c) that large μ_i values lead to large control gains in $\boldsymbol{k}$ increasing the risk of actuator saturation. Hence, the choice of appropriate μ_i is a compromise between the speed of convergence and reducing the risk of actuator saturation. Furthermore, large λ_is can result in huge $|s_i(0)|$ for nonzero initial errors (see (4)) which may lead to large convergence times as $l_i(0) = s_i(0) - \phi_i \,\mathrm{sat}(s_i(0)/\phi_i)$.

5 Trajectory Tracking Control of the URV

5.1 Problem Formulation

The goal of this section is to derive a robust control law $\boldsymbol{\tau} \in \mathbb{R}^3$ so that that the actual pose $\boldsymbol{\eta} = [x(t), y(t), \varphi(t)]^T$ of the URV (1) with hydrodynamic parametric uncertainties can track a desired time varying trajectory $\boldsymbol{\eta}_d = [x_d(t), y_d(t), \varphi_d(t)]^T$

with each $\boldsymbol{\eta_d}[i], \forall i \in \mathbb{L} = \{1, 2, 3\}$ satisfying *Assumption 2*. The derived control law should guarantee the boundedness of all the closed-loop signals and converge the tracking error $\boldsymbol{e} = \boldsymbol{\eta} - \boldsymbol{\eta}_d \in \mathbb{R}^3$ to a neighborhood of the origin that can be made arbitrarily small.

5.2 Control Law Derivation

Considering (1b) and the definitions of its terms, we can obtain that

$$\dot{\boldsymbol{\upsilon}} = \boldsymbol{\mathfrak{h}} + \boldsymbol{\mathcal{A}}\boldsymbol{\tau}, \tag{20}$$

where

$$\boldsymbol{\mathfrak{h}} = \Big[\frac{m_2}{m_1} rv - \frac{c_1}{m_1}u, -\frac{m_1}{m_2} ru - \frac{c_2}{m_2}v, \frac{m_1 - m_2}{m_3}uv - \frac{c_3}{m_3}r\Big]^T,$$

and $\boldsymbol{\mathcal{A}} = \text{diag}(1/m_1, 1/m_2, 1/m_3)\boldsymbol{B}$. Here we shall make the following assumption.

Assumption 5: Inertia terms m_i and drag coefficients c_i are unknown but positive and bounded: $m_i = \widehat{m}_i + \delta m_i$ with $|\delta m_i| \leq \overline{\delta m_i} < \widehat{m}_i$ and $c_i = \widehat{c}_i + \delta c_i$ with $|\delta c_i| \leq \overline{\delta c}_i < \widehat{c}_i, \forall i \in \mathbb{L}$. $\overline{\delta m}_i$ and $\overline{\delta c}_i$ are known bounds of uncertainties δm_i and δc_i respectively.

We can obtain $\widehat{\boldsymbol{\mathcal{A}}}$ considering *Assumption 5*. Also, it is worth noting that the structure of $\boldsymbol{\mathcal{A}}$ guarantees the invertibility of both $\boldsymbol{\mathcal{A}}$ and $\widehat{\boldsymbol{\mathcal{A}}}$. Time differentiating (1a) and using (20), we obtain an alternative version of the URV model as

$$\ddot{\boldsymbol{\eta}} = \boldsymbol{R}\boldsymbol{\mathfrak{h}} + \dot{\boldsymbol{R}}\boldsymbol{\upsilon} + \boldsymbol{R}\boldsymbol{\mathcal{A}}\boldsymbol{\tau}. \tag{21}$$

Similar to *Assumption 1*, if $\boldsymbol{\eta}$ and $\dot{\boldsymbol{\eta}}$ are assumed to be available, we can obtain $\boldsymbol{\upsilon}$ noting that $\boldsymbol{\upsilon} = \boldsymbol{R}^{-1}\dot{\boldsymbol{\eta}} = \boldsymbol{R}^T\dot{\boldsymbol{\eta}}$. So, it can be concluded that the terms $\boldsymbol{R}\boldsymbol{\mathfrak{h}}$, $\dot{\boldsymbol{R}}\boldsymbol{\upsilon}$, and $\boldsymbol{R}\boldsymbol{\mathcal{A}}$ in (21) are analogous to $\boldsymbol{h}$, $\boldsymbol{q}$, and $\boldsymbol{A}$ in (2) respectively complying with their definitions. Since $\boldsymbol{\upsilon}$ is available, we can now obtain $\widehat{\boldsymbol{\mathfrak{h}}}$ considering *Assumption 5*.

Proposition 1: Consider $p, q > 0$ such that $p = \widehat{p} + \delta p$ with $|\delta p| \leq \overline{\delta p} < \widehat{p}$ and $q = \widehat{q} + \delta q$ with $|\delta q| \leq \overline{\delta q} < \widehat{q}$. Then,

$$\frac{p}{q} - \frac{\widehat{p}}{\widehat{q}} = \frac{\widehat{p}}{\widehat{q}}\Big\{\frac{\delta p}{\widehat{p}} - \frac{\delta q}{\widehat{q}}\Big(1 + \frac{\delta p}{\widehat{p}}\Big)/\Big(1 + \frac{\delta q}{\widehat{q}}\Big)\Big\},$$

and further $\Big|\frac{p}{q} - \frac{\widehat{p}}{\widehat{q}}\Big| \leq \mathcal{J}\Big(\frac{\widehat{p}}{\widehat{q}}\Big)$ where

$$\mathcal{J}\Big(\frac{\widehat{p}}{\widehat{q}}\Big) = \frac{\widehat{p}}{\widehat{q}}\Big\{\frac{\overline{\delta p}}{\widehat{p}} + \frac{\overline{\delta q}}{\widehat{q}}\Big(1 + \frac{\overline{\delta p}}{\widehat{p}}\Big)/\Big(1 - \frac{\overline{\delta q}}{\widehat{q}}\Big)\Big\}.$$

Proof: $\dfrac{p}{q} = \dfrac{\widehat{p}+\delta p}{\widehat{q}+\delta q} = \dfrac{\widehat{p}}{\widehat{q}}\Big(1+\dfrac{\delta p}{\widehat{p}}\Big)(1+\Gamma)$ where

$$\Gamma = \sum_{k=1}^{\infty}\Big(-\frac{\delta q}{\widehat{q}}\Big)^k = -\frac{\delta q}{\widehat{q}}\Big/\Big(1+\frac{\delta q}{\widehat{q}}\Big),$$

since $|\delta q| < \widehat{q}$. Then, we have $\dfrac{p}{q} - \dfrac{\widehat{p}}{\widehat{q}} = \dfrac{\widehat{p}}{\widehat{q}}\Big\{\dfrac{\delta p}{\widehat{p}} + \Big(1+\dfrac{\delta p}{\widehat{p}}\Big)\Gamma\Big\}$ with which the rest of the proof is straightforward.

Using *Assumption 5* and *Proposition 1*, we can derive that

$$\boldsymbol{\mathcal{A}} - \widehat{\boldsymbol{\mathcal{A}}} = \boldsymbol{\mathcal{E}}\widehat{\boldsymbol{\mathcal{A}}}, \tag{22}$$

where $\boldsymbol{\mathcal{E}} = \text{diag}(\mathcal{E}_1, \mathcal{E}_2, \mathcal{E}_3)$ with $\mathcal{E}_i = -\dfrac{\delta m_i}{\widehat{m}_i}\Big/\Big(1+\dfrac{\delta m_i}{\widehat{m}_i}\Big), \forall i \in \mathbb{L}$. Further, we define $\boldsymbol{\mathcal{D}} = \text{diag}(\mathcal{D}_1, \mathcal{D}_2, \mathcal{D}_3)$ with $\mathcal{D}_i = \dfrac{\overline{\delta m}_i}{\widehat{m}_i}\Big/\Big(1-\dfrac{\overline{\delta m}_i}{\widehat{m}_i}\Big)$ such that $|\boldsymbol{\mathcal{E}}[i,i]| \leq \boldsymbol{\mathcal{D}}[i,i], \forall i \in \mathbb{L}$. So, in general, we can say that $|\boldsymbol{\mathcal{E}}[i,j]| \leq \boldsymbol{\mathcal{D}}[i,j], \forall i,j \in \mathbb{L}$. Let's consider $\boldsymbol{\delta\mathfrak{h}} \in \mathbb{R}^3$ defined as

$$\boldsymbol{\delta\mathfrak{h}} = \begin{bmatrix} \mathcal{J}\Big(\dfrac{\widehat{m}_2}{\widehat{m}_1}\Big)|rv| + \mathcal{J}\Big(\dfrac{\widehat{c}_1}{\widehat{m}_1}\Big)|u| \\ \mathcal{J}\Big(\dfrac{\widehat{m}_1}{\widehat{m}_2}\Big)|ru| + \mathcal{J}\Big(\dfrac{\widehat{c}_2}{\widehat{m}_2}\Big)|v| \\ \mathcal{J}\Big(\dfrac{\widehat{m}_1}{\widehat{m}_3}\Big)|uv| + \mathcal{J}\Big(\dfrac{\widehat{m}_2}{\widehat{m}_3}\Big)|uv| + \mathcal{J}\Big(\dfrac{\widehat{c}_3}{\widehat{m}_3}\Big)|r| \end{bmatrix}, \tag{23}$$

with $\mathcal{J}(\cdot)$ defined in *Proposition 1*. It can be seen from *Assumption 5* and *Proposition 1* that $|\mathfrak{h}[i] - \widehat{\mathfrak{h}}[i]| \leq \boldsymbol{\delta\mathfrak{h}}[i]$.

Regarding the system given by (21), we can design sliding surfaces S_x, S_y, and S_φ and associated boundary layers L_x, L_y, and L_φ with appropriate thicknesses ϕ_x, ϕ_y, $\phi_\varphi > 0$ as described for the model system considered in (2). Then, for the system in (21), we can easily deduce from (6) that

$$\dot{\boldsymbol{s}} = \boldsymbol{R}\boldsymbol{\mathfrak{h}} + \dot{\boldsymbol{R}}\boldsymbol{v} - \boldsymbol{\gamma} + \boldsymbol{\Lambda}\dot{\boldsymbol{e}} + \boldsymbol{R}\boldsymbol{\mathcal{A}}\boldsymbol{\tau}, \tag{24}$$

where $\boldsymbol{s} = [s_x, s_y, s_\varphi]^T$ which is the vector containing the distances from the error states to the sliding surfaces, $\boldsymbol{\gamma} = \ddot{\boldsymbol{\eta}}_d$, $\boldsymbol{\Lambda} = \text{diag}(\lambda_x, \lambda_y, \lambda_\varphi)$ with $\boldsymbol{\Lambda}[i,i] > 0, \forall i \in \mathbb{L}$, and $\boldsymbol{e} = [e_x, e_y, e_\varphi]^T$. Let the feedback control law be defined as

$$\boldsymbol{\tau} = \widehat{\boldsymbol{\mathcal{A}}}^{-1}\boldsymbol{R}^T(\boldsymbol{f} - \boldsymbol{\Psi}\boldsymbol{k}), \tag{25a}$$

$$\boldsymbol{f} = -\boldsymbol{R}\widehat{\boldsymbol{\mathfrak{h}}} - \dot{\boldsymbol{R}}\boldsymbol{v} + \boldsymbol{\gamma} - \boldsymbol{\Lambda}\dot{\boldsymbol{e}}, \tag{25b}$$

$$\boldsymbol{k} = (\boldsymbol{I} - \boldsymbol{\mathcal{R}}\boldsymbol{\mathcal{D}}\boldsymbol{\mathcal{R}})^{-1}\Big(\boldsymbol{\mathcal{R}}\big(\boldsymbol{\delta\mathfrak{h}} + \boldsymbol{\mathcal{D}}\boldsymbol{\mathcal{R}}|\overrightarrow{\boldsymbol{f}}|\big) + \boldsymbol{\mu}\Big), \tag{25c}$$

with

$$\boldsymbol{\mathcal{R}}[i,j] = |\boldsymbol{R}[i,j]|, \forall i,j \in \mathbb{L}. \tag{26}$$

In (25), $\boldsymbol{\Psi} = \text{diag}\big(\text{sat}(s_x/\phi_x), \text{sat}(s_y/\phi_y), \text{sat}(s_\varphi/\phi_\varphi)\big)$ with $\text{sat}(\cdot)$ defined in (8), $\boldsymbol{\mu} = [\mu_x, \mu_y, \mu_\varphi]^T$ with $\boldsymbol{\mu}[i] > 0, \forall i \in \mathbb{L}$, and $\boldsymbol{I} \in \mathbb{R}^{3\times 3}$ is the identity matrix. In *Corollary 1*, we will prove the feasibility of the controller (25) to achieve the desired trajectory tracking retaining stable closed-loop dynamics.

Corollary 1: Let the URV be represented by (21). Then, subject to *Assumption 5*, the controller defined by (25) ensures the desired trajectory tracking formulated in Section 5.1 if $\overline{\delta m_i}/\widehat{m}_i < 1/3, \forall i \in \mathbb{L}$.

Proof: Comparing the terms of (6) and (24), it follows from (7a) and (7b) that the candidate $\boldsymbol{\tau}$ for (21) has the form

$$\boldsymbol{\tau} = (\boldsymbol{R}\widehat{\boldsymbol{\mathcal{A}}})^{-1}(\boldsymbol{f} - \boldsymbol{\Psi k}) = \widehat{\boldsymbol{\mathcal{A}}}^{-1}\boldsymbol{R}^T(\boldsymbol{f} - \boldsymbol{\Psi k}), \tag{27}$$

$$\boldsymbol{f} = -\boldsymbol{R}\widehat{\mathfrak{h}} - \dot{\boldsymbol{R}}\boldsymbol{v} + \boldsymbol{\gamma} - \boldsymbol{\Lambda}\dot{\boldsymbol{e}}, \tag{28}$$

where $\boldsymbol{\Psi} = \text{diag}\big(\text{sat}(s_x/\phi_x), \text{sat}(s_y/\phi_y), \text{sat}(s_\varphi/\phi_\varphi)\big)$ and $\boldsymbol{k} \in \mathbb{R}^3$ is to be determined. Noting that $\boldsymbol{\mathcal{A}}\widehat{\boldsymbol{\mathcal{A}}}^{-1} = \boldsymbol{I} + \boldsymbol{\mathcal{E}}$ from (22) and $\boldsymbol{R}\boldsymbol{R}^T = \boldsymbol{I}$ where $\boldsymbol{I} \in \mathbb{R}^{3\times 3}$ is identity matrix, we see that substituting expressions for $\boldsymbol{\tau}$ and $\boldsymbol{f}$ into (24) yields

$$\dot{\boldsymbol{s}} = \boldsymbol{R}(\mathfrak{h} - \widehat{\mathfrak{h}}) - \boldsymbol{\Psi k} + \boldsymbol{R}\boldsymbol{\mathcal{E}}\boldsymbol{R}^T(\boldsymbol{f} - \boldsymbol{\Psi k}). \tag{29}$$

When this is compared to (14), we observe that $\boldsymbol{R}(\mathfrak{h} - \widehat{\mathfrak{h}})$ and $\boldsymbol{R}\boldsymbol{\mathcal{E}}\boldsymbol{R}^T$ are analogous to $\boldsymbol{h} - \widehat{\boldsymbol{h}}$ and $\boldsymbol{\Delta}$ respectively. From *Assumption 3* and *4*, the elements of $\boldsymbol{h} - \widehat{\boldsymbol{h}}$ and $\boldsymbol{\Delta}$ are bounded as $\boldsymbol{\delta h}[i] \geq |h_i - \widehat{h}_i|$ and $\boldsymbol{D}[i,j] \geq |\Delta_{ij}|$ with $\|\boldsymbol{D}\|_2 < 1$. We can find similar bounding functions for elements in $\boldsymbol{R}(\mathfrak{h} - \widehat{\mathfrak{h}})$ and $\boldsymbol{R}\boldsymbol{\mathcal{E}}\boldsymbol{R}^T$ as follows. Referring to (23) and (26), we can find $\boldsymbol{p} = \boldsymbol{\mathcal{R}}\boldsymbol{\delta\mathfrak{h}}$ such that $\boldsymbol{p}[i] \geq |\boldsymbol{z}[i]|, \forall i \in \mathbb{L}$ where $\boldsymbol{z} = \boldsymbol{R}(\mathfrak{h} - \widehat{\mathfrak{h}})$ indicating the analogy between $\boldsymbol{\delta h}$ and $\boldsymbol{\mathcal{R}}\boldsymbol{\delta\mathfrak{h}}$. Recalling that $\boldsymbol{D}[i,j] \geq |\boldsymbol{\mathcal{E}}[i,j]|$, we can find $\boldsymbol{P} = \boldsymbol{\mathcal{R}}\boldsymbol{\mathcal{D}}\boldsymbol{\mathcal{R}}^T = \boldsymbol{\mathcal{R}}\boldsymbol{\mathcal{D}}\boldsymbol{\mathcal{R}}$ such that $\boldsymbol{P}[i,j] \geq |\boldsymbol{Z}[i,j]|, \forall i,j \in \mathbb{L}$ where $\boldsymbol{Z} = \boldsymbol{R}\boldsymbol{\mathcal{E}}\boldsymbol{R}^T$. However, in order for $\boldsymbol{\mathcal{R}}\boldsymbol{\mathcal{D}}\boldsymbol{\mathcal{R}}$ to be analogous to $\boldsymbol{D}$, the following condition should be satisfied.

$$\|\boldsymbol{\mathcal{R}}\boldsymbol{\mathcal{D}}\boldsymbol{\mathcal{R}}\|_2 < 1. \tag{30}$$

Since matrix 2-norm is submultiplicative, we have $\|\boldsymbol{\mathcal{R}}\boldsymbol{\mathcal{D}}\boldsymbol{\mathcal{R}}\|_2 \leq (\|\boldsymbol{\mathcal{R}}\|_2)^2\|\boldsymbol{\mathcal{D}}\|_2$. Further, singular values of $\boldsymbol{\mathcal{R}}$ can be easily shown to be $1, \sqrt{1-\sin(2\varphi)}$, and $\sqrt{1+\sin(2\varphi)}$ which yield a maximum singular value of $\sqrt{2}$ i.e., $\|\boldsymbol{\mathcal{R}}\|_2 = \sqrt{2}$ when $\sin 2\varphi = \pm 1$. The condition (30) is sufficiently satisfied if $(\|\boldsymbol{\mathcal{R}}\|_2)^2\|\boldsymbol{\mathcal{D}}\|_2 < 1$. Accordingly, for all possible rotations, we should have $\|\boldsymbol{\mathcal{D}}\|_2 < 1/2$. Since $\boldsymbol{\mathcal{D}}$ is diagonal, its singular values are its diagonal elements themselves. So, $\|\boldsymbol{\mathcal{D}}\|_2 < 1/2$ always holds true when $\dfrac{\overline{\delta m_i}}{\widehat{m}_i}\Big/\Big(1 - \dfrac{\overline{\delta m_i}}{\widehat{m}_i}\Big) < 1/2$ or equivalently $\overline{\delta m_i}/\widehat{m}_i < 1/3, \forall i \in \mathbb{L}$. From above arguments, we have $\boldsymbol{\mathcal{R}}\boldsymbol{\delta\mathfrak{h}}$ and $\boldsymbol{\mathcal{R}}\boldsymbol{\mathcal{D}}\boldsymbol{\mathcal{R}}$ analogous to $\boldsymbol{\delta h}$ and $\boldsymbol{D}$ respectively. Considering these analogies, we can now write the appropriate control gain vector $\boldsymbol{k}$ from (7c) as

$$\boldsymbol{k} = (\boldsymbol{I} - \boldsymbol{\mathcal{R}}\boldsymbol{\mathcal{D}}\boldsymbol{\mathcal{R}})^{-1}\Big(\boldsymbol{\mathcal{R}}\big(\boldsymbol{\delta\mathfrak{h}} + \boldsymbol{\mathcal{D}}\boldsymbol{\mathcal{R}}|\overrightarrow{\boldsymbol{f}}|\big) + \boldsymbol{\mu}\Big), \tag{31}$$

where $\boldsymbol{f}$ is given by (28) and $\boldsymbol{\mu} \in \mathbb{R}^3$ with $\boldsymbol{\mu}[i] > 0, \forall i \in \mathbb{L}$. We observe that the deduced control law in (27), (28), and (31) is equivalent to the control law given by (25). Further, we can state that the system (21) is now fit for *Theorem 1* to be applied (observe that through the results which stem from *Assumption 5* and the constraint $\overline{\delta m_i}/\widehat{m}_i < 1/3, \forall i \in \mathbb{L}$, the system (21) complies with *Assumption 3* and *4* whereas *Assumption 1* and *2* are already assumed to be met earlier in this section). So, it follows from *Theorem 1* and *Lemma 3* that the desired trajectory tracking is achieved completing the proof.

Remark 7: Corollary 1 establishes the conditions which should be satisfied by hydrodynamic parameters uncertainties in order to guarantee the global closed-loop stability. Although no constraint is enforced on $|\delta c_i|$, we restrict our analysis to $|\delta c_i| < \widehat{c}_i$ simply to avoid actuator saturation which otherwise would be likely due to large control gains. To summarize, the uncertainty in c_i should be bounded as $|\delta c_i| \leq \overline{\delta c}_i < \widehat{c}_i$ whereas the uncertainty in m_i should be bounded as $|\delta m_i| \leq \overline{\delta m}_i < \widehat{m}_i/3, \forall i \in \mathbb{L}$.

6 Simulation Results

We simulate the performance of the derived MIMO sliding mode controller (25) and its extendibility to control URVs belonging to the specific class mentioned in *Remark 8*. All the simulations are performed with discrete implementations of (21) and (25) in MATLAB at a sampling rate of 20Hz.

First, in order to evaluate the controller performance, a simulation is performed based on the URV's dynamic model (21) which has coupled dynamics and the obtained results are presented in Fig. 5 and Fig. 6. The controller's competence to steer the URV to track a predefined trajectory subject to hydrodynamic parameter uncertainties is illustrated. The parameter estimates used in the simulation are given in Section 3.2. The chosen tunable parameters are $\lambda_x = \lambda_y = \lambda_\varphi = 2.5$, $\phi_x = \phi_y = \phi_\varphi = 0.5$, and $\mu_x = \mu_y = \mu_\varphi = 0.01$. Hydrodynamic parameter uncertainties are considered to be bounded by $\pm 10\%$ of the corresponding parameter estimates so that the conditions on uncertainty bounds are met. For the dynamic model, the chosen values are $m_1 = 22$ kg, $m_2 = 23$ kg, $m_3 = 0.21$ kg.m^2, $c_1 = 36$ kg/s, $c_2 = 31.5$ kg/s, and $c_3 = 3.3$ kg.m^2/s. Regarding the reference trajectory, a circular trajectory defined as $x_d(t) = 3\cos(t/15)$, $y_d(t) = 3\sin(t/15)$, and $\varphi_d(t) = \pi/2 + t/15$ is considered. The initial states of the URV are chosen as $\boldsymbol{\eta}(0) = [1, -1, \pi/3]^T$ and $\dot{\boldsymbol{\eta}}(0) = [0, 0, 0]^T$. The time evolution of s_x, s_y, and s_φ are shown in Fig. 5(a). All the trajectories start outside the boundary layer and converge inside it by $t = t_r = 18$ s. The tracking errors are depicted in Fig. 5(b) and we observe that they converge to close neighborhoods of zero which are in side the error margin $|e_x| = |e_y| = |e_\varphi| = 0.2$ complying with *Lemma 3*. The mean absolute errors (MAEs) of e_x, e_y, and e_φ within $t = 40$ s and $t = 100$ s are found to be 0.010 m, 0.012 m, and 0.015 rad respectively per pose and therefore can be considered satisfactorily small. The SMC thrust forces are presented in Fig. 5(c) and we observe that they are within

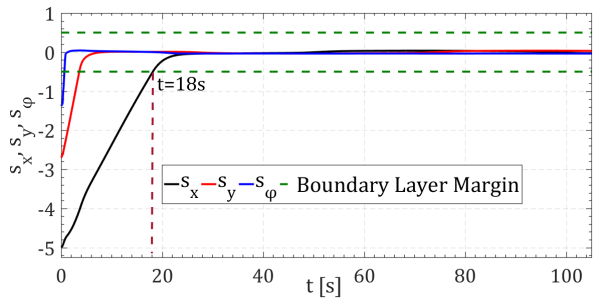

(a)

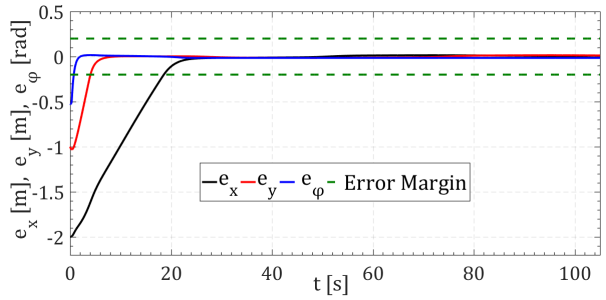

(b)

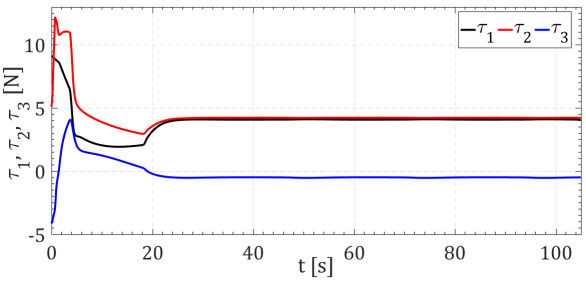

(c)

Fig. 5 *Trajectory tracking of the URV*
(**a**) Time evolution of s_x,s_y, and s_φ, (**b**) Tracking errors under SMC, (**c**) SMC thrust forces

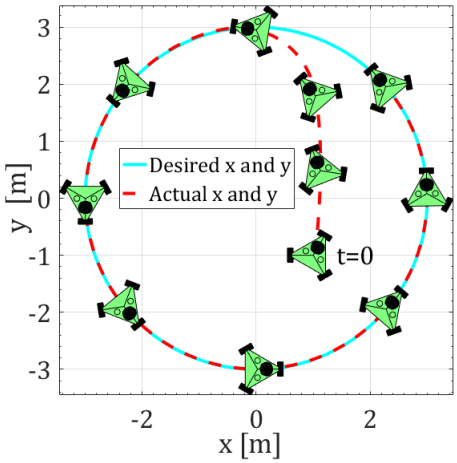

Fig. 6 *Spatial evolution of the URV's pose under SMC*

the operating limits of the thrusters given in Table 1. Also, the chattering phenomenon is completely absent. Hence, under the chosen tunable parameters, the SMC closed-loop system performs well. Otherwise, these parameters should be reselected considering Remark 5 and 6. The evolution of the robot's pose in 2D space under SMC is illustrated in Fig. 6 and we observe that the desired geometric shape of the trajectory is well achieved.

References

[1] Bessa, W.M., Dutra, M.S., Kreuzer, E.: 'Depth control of remotely operated underwater vehicles using an adaptive fuzzy sliding mode controller', Rob. Auton. Syst., 2008, 56, (8), pp. 670–677

[2] Chen, M., Mei, R., Jiang, B.: 'Sliding mode control for a class of uncertain MIMO nonlinear systems with application to near-space vehicles', Math. Probl. Eng., 2013, pp. 1–9.

[3] Fossen, T.I., et al.: 'Guidance and control of ocean vehicles' (Wiley, New York, 1994)

[4] Chin, C.S.: 'Computer-Aided Control Systems Design: Practical Applications Using MATLAB® and Simulink®' (CRC Press, Boca Raton, FL, 2012)

[5] Lihua, S.: 'Calculation of added mass for underwater vehicles based on FVM'. Proc. Int. Conf. on Advances in Mechanical Engineering and Industrial Informatics, Hangzhou, Zhejiang, 2016, pp. 969–974

[6] Slotine, J.J.E., Li, W., et al.: 'Applied nonlinear control' (Prentice Hall Englewood Cliffs, NJ, 1991)